

Welcome to the Twilight Zone: The Mid-Infrared Properties of Post-starburst Galaxies

Katherine Alatalo,^{1†} Theodoros Bitsakis,² Lauranne Lanz,^{3,4} Mark Lacy,⁵ Michael J. I. Brown,^{6,7‡} K. Decker French,⁸ Laure Ciesla,⁹ Philip N. Appleton,⁵ Rachael L. Beaton,¹ Sabrina L. Cales,¹⁰ Jacob Crossett,⁶ Jesús Falcón-Barroso,^{11,12} Daniel D. Kelson,¹ Lisa J. Kewley,¹³ Mariska Kriek,¹⁴ Anne M. Medling,^{13,15†} John S. Mulchaey,¹ Kristina Nyland,⁵ Jeffrey A. Rich,¹ & C. Meg Urry¹⁰

¹Observatories of the Carnegie Institution of Washington, 813 Santa Barbara Street, Pasadena, CA 91101, USA

²Instituto de Radioastronomía y Astrofísica, Universidad Nacional Autónoma de México, C.P. 58190, Morelia, Mexico

³Infrared Processing and Analysis Center, California Institute of Technology, Pasadena, California 91125, USA

⁴National Radio Astronomy Observatory, 520 Edgemont Road, Charlottesville, VA 22903, USA

⁵Dartmouth College, 6127 Wilder Laboratory, Hanover, NH 03755, USA

⁶School of Physics, Monash University, Clayton, Victoria 3800, Australia

⁷Monash Centre for Astrophysics, Monash University, Clayton, Victoria 3800, Australia

⁸Steward Observatory, University of Arizona, 933 North Cherry Avenue, Tucson, AZ 85721, USA

⁹Laboratoire AIM-Paris-Saclay, CEA/DSM/Irfu - CNRS - Université Paris Diderot, CEA-Saclay, F-91191 Gif-sur-Yvette, France

¹⁰Yale Center for Astronomy and Astrophysics, Physics Department, Yale University, New Haven, CT 06511 USA

¹¹Instituto de Astrofísica de Canarias, E-38205 La Laguna, Tenerife, Spain

¹²Departamento de Astrofísica, Universidad de La Laguna (ULL), E-38200 La Laguna, Tenerife, Spain

¹³Research School of Astronomy and Astrophysics, Australian National University, Cotter Rd., Weston ACT 2611, Australia

¹⁴Department of Astronomy, Campbell Hall, University of California, Berkeley, CA 94720, USA

¹⁵California Institute of Technology, MC 249-17, 1200 East California Boulevard, Pasadena, CA 91125, USA

Accepted to the *Astrophysical Journal*, May 11, 2017

ABSTRACT

We investigate the optical and *Wide-field Survey Explorer* (*WISE*) colors of “E+A” identified post-starburst galaxies, including a deep analysis on 190 post-starbursts detected in the $2\mu\text{m}$ All Sky Survey Extended Source Catalog. The post-starburst galaxies appear in both the optical green valley and the *WISE* Infrared Transition Zone (IRTZ). Furthermore, we find that post-starbursts occupy a distinct region $[3.4]\text{--}[4.6]$ vs. $[4.6]\text{--}[12]$ *WISE* colors, enabling the identification of this class of transitioning galaxies through the use of broad-band photometric criteria alone. We have investigated possible causes for the *WISE* colors of post-starbursts by constructing a composite spectral energy distribution (SED), finding that mid-infrared ($4\text{--}12\mu\text{m}$) properties of post-starbursts are consistent with either $11.3\mu\text{m}$ polycyclic aromatic hydrocarbon emission, or Thermally Pulsating Asymptotic Giant Branch (TP-AGB) and post-AGB stars. The composite SED of extended post-starburst galaxies with $22\mu\text{m}$ emission detected with signal to noise ≥ 3 requires a hot dust component to produce their observed rising mid-infrared SED between 12 and $22\mu\text{m}$. The composite SED of *WISE* $22\mu\text{m}$ non-detections ($S/N < 3$), created by stacking $22\mu\text{m}$ images, is also flat, requiring a hot dust component. The most likely source of this mid-infrared emission of these E+A galaxies is a buried active galactic nucleus. The inferred upper limit to the Eddington ratios of post-starbursts are $10^{-2}\text{--}10^{-4}$, with an average of 10^{-3} . This suggests that AGNs are not radiatively dominant in these systems. This could mean that including selections able to identify active galactic nuclei as part of a search for transitioning and post-starburst galaxies would create a more complete census of the transition pathways taken as a galaxy quenches its star formation.

Keywords: galaxies: evolution — galaxies: star formation – galaxies: stellar content – infrared: galaxies

1. INTRODUCTION

Galaxies in the modern universe show two bimodal distributions, one in morphology and one in color space. In morphology space, a “tuning fork” has been used to classify galaxies since Hubble (1926), representing spiral (late-type) galaxies and elliptical and lenticular (early-type) galaxies. In color space, galaxies break into a blue cloud and a red sequence (Baade 1958; Holmberg 1958; Tinsley 1978; Strateva et al. 2001; Baldry et al. 2004), with a genuine dearth of galaxies with intermediate colors in the so-called “green valley.” This dearth is used to suggest that galaxies undergoing the metamorphosis between blue spirals and red early-types must be rapid.

kalatalo@carnegiescience.edu

[†] Hubble fellow

[‡] Future ARC fellow

Once $z \approx 0$ galaxies begin the process of transitioning, the probability that it is a one-way process is high (Appleton et al. 2013; Young et al. 2014), with very few circumstances in which the galaxy will transition back permanently (Kannappan et al. 2013). Because of this, it is essential to understand all possible pathways and physical mechanisms that can trigger a galaxy’s metamorphosis. Many pathways to transformation have been observed, though it is likely that the list is not exhaustive.

Mergers are capable of driving the molecular gas into the center, allowing it to be consumed in a starburst, and heating the stellar disks of the interacting galaxies (Toomre & Toomre 1972; Springel et al. 2005), creating an elliptical galaxy. Minor mergers also appear capable of quenching star formation (Qu et al. 2010; Eliche-Moral et al. 2012; Alatalo et al. 2014a), especially if the recipient galaxy endures many minor mergers over its lifetime. Secular evolution, in which a

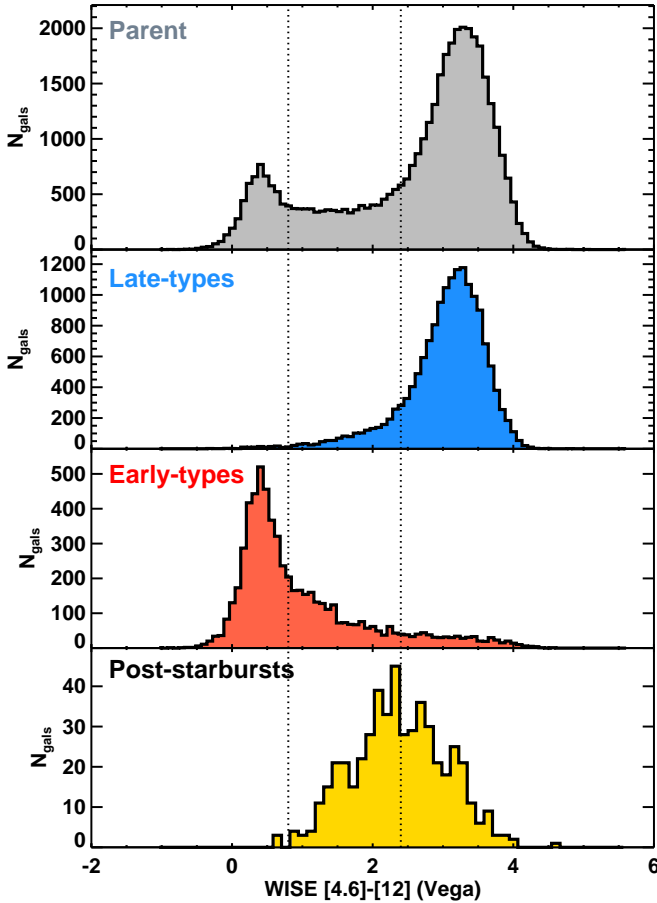


Figure 1. The $[4.6]–[12]$ *WISE* color distributions of the various samples, including the Galaxy Zoo comparison sample of early-type and late-type galaxies (Schawinski et al. 2014; Alatalo et al. 2014b; gray, top) delineated between late-type galaxies (blue) and early-type galaxies (red), with the redshift-corrected post-starburst galaxy colors for comparison (yellow). The boundaries of the IRTZ are shown as a striped line through all plots. Post-starburst galaxies peak on the star-forming side of the IRTZ, and have the highest fractional IRTZ representation of the galaxies shown.

galaxy bulge grows sufficiently large to stabilize a molecular disk against gravitational collapse (thus inhibiting star formation) has also been shown in simulations to quench galaxies (Martig et al. 2009), with additional observational evidence manifesting in early-type galaxies (Martig et al. 2013; Davis et al. 2014).

When galaxies fall into a cluster potential, they suffer strangulation, in which their ability to accrete external gas and replenish their supply is stunted (Bekki et al. 2002; Blanton & Moustakas 2009), truncating star formation. They can also suffer harassment, in which gravitational torques from other cluster members dynamically heat the stars (Mihos 1995; Moore et al. 1996; Bekki 1998). Group interactions (Hickson et al. 1992; Zabludoff & Mulchaey 1998) are able to catalyze quenching, which has been observed through the study of the individual group galaxies (Johnson et al. 2007; Bitsakis et al. 2011, 2014, 2016; Martinez-Badenes et al. 2012; Lisenfeld et al. 2014; Alatalo et al. 2015b) and the evolution of the intragroup medium (Verdes-Montenegro et al. 2001; Rasmussen et al. 2008; Borthakur et al. 2010). Additionally, it is possible that much of the galaxy transformation observed in the cluster environment takes place during a group pre-processing phase (Dressler et al. 2013).

Active Galactic Nucleus (AGN) feedback, introduced

to explain the truncated mass function of galaxies (Silk & Rees 1998; Di Matteo et al. 2005; Croton et al. 2006; Oppenheimer et al. 2010) can rapidly expel star-forming fuel from the galaxy and quickly quench star formation (Hopkins et al. 2006, 2008). Molecular gas outflows detected in some AGN hosts may be a signature of AGN feedback (Fischer et al. 2010; Feruglio et al. 2010; Sturm et al. 2011; Alatalo et al. 2011; Aalto et al. 2012, 2016; Ciccone et al. 2012, 2014), though the nearby examples do not appear to be powerful enough to rapidly eject the interstellar medium from the host, instead mainly injecting turbulence into the existing gas (Alatalo et al. 2015a; Guillard et al. 2015; Lanz et al. 2015, 2016; Costagliola et al. 2016) and ultimately depleting molecular gas at a rate consistent with the star formation rate (Alatalo 2015). It is possible that radiation-mode AGN feedback provides sufficient energy to quench a galaxy at high redshift (Zakamska et al. 2016), but the mechanism does not appear to be common in the modern universe. It is likely that the pathways discussed above are not an exhaustive sample; therefore creating a large sample of galaxies undergoing this transformation is necessary to probe the various conditions that can trigger it, possibly identifying new pathways that lead a galaxy to evolve.

Despite the color and morphology bimodalities, finding galaxies that are rapidly transitioning is more complicated than determining their colors and morphologies. Schawinski et al. (2014) showed that the number of galaxies within the green valley undergoing morphological change is small compared to galaxies whose intermediate colors are caused by secular processes, in which normal spiral galaxies with normal star-forming histories build up a substantial population of lower mass (redder) stars with a constant star formation rate, gradually turning the integrated colors of the galaxy green.

More recently, a mid-infrared (mid-IR) color bimodality was observed using the *Wide-field Infrared Survey Explorer* (*WISE*; Wright et al. 2010). Authors identified a bimodality in both the $[3.4]–[12]\mu\text{m}$ (Ko et al. 2013, 2016) as well as the $[4.6]–[12]\mu\text{m}$ colors (Yesuf et al. 2014; Alatalo et al. 2014b). In the case of the $[4.6]–[12]$ colors, Alatalo et al. (2014b) showed that color bimodality not only split based on galaxy morphology but that it was also more prominent than optical colors, and termed it the “infrared transition zone” (IRTZ).

Post-starburst galaxies are one such sample that have robustly been shown to have undergone a rapid cessation of star formation (Dressler & Gunn 1983; Zabludoff et al. 1996) via the presence of stellar absorption features consistent with intermediate stellar populations (such as strong Balmer absorption; Vazdekis et al. 2010) and a lack of nebular ionized gas emission, such as $\text{H}\alpha$ or $[\text{O II}]\lambda 3727$, which originates from H II regions associated with current (within the last 10 Myr) star formation. These methods include the “K+A” method, which uses a weighting of A-star and K-star stellar libraries to determine a young star fraction (Dressler & Gunn 1983; Quintero et al. 2004) or a “E+A” identification (an early-type galaxy with A-type stars), which relies on Balmer absorption identification (Goto 2005, 2007). Although it is likely that the stringent selections used to pinpoint post-starburst galaxies miss a non-negligible fraction of transitioning galaxies, including those that host quasars (Canalizo & Stockton 2000, 2013; Cales et al. 2011, 2013; Cales & Brotherton 2015) or shocks (Davis et al. 2012; Alatalo et al. 2014a,b, 2016a), they are a bonafide sample of transitioning galaxies.

We utilize the post-starburst sample compiled by Goto

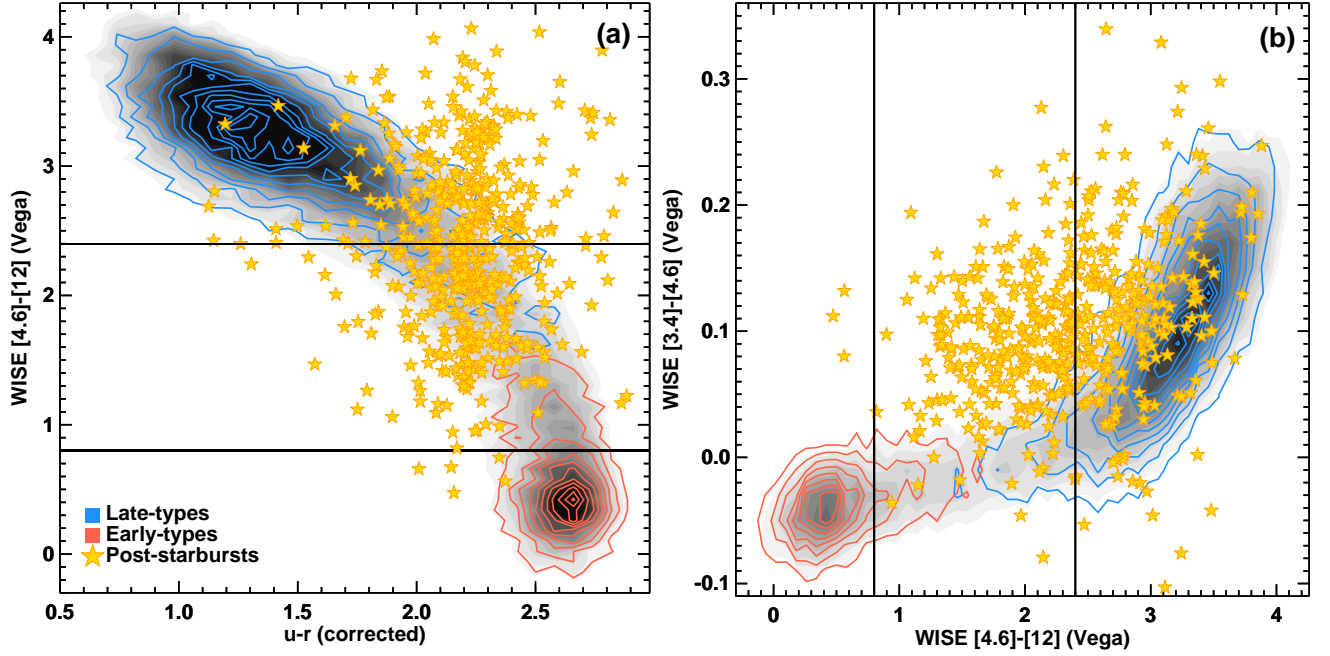


Figure 2. (Left): The $u-r$ vs. redshift-corrected $[4.6]-[12]$ colors show a strong correlation with the prominent separation between late-types (blue contours) and early-types (red contours) from Schawinski et al. (2014). Post-starbursts (yellow stars) are located right between the two populations. (Right): $[4.6]-[12]$ vs. $[3.4]-[4.6]$ WISE colors, which show that the post-starburst galaxies have slightly elevated $[3.4]-[4.6]$ colors compared to the Galaxy Zoo sample. Post-starbursts have colors that are consistent with the Seyfert sample shown in Alatalo et al. (2014b). The IRTZ is shown as black solid lines in each plot. The optical colors are k -corrected. The mid-IR colors are redshift corrected (see §2.2).

(2007) to probe various properties of transitioning galaxies, including whether the *WISE* colors and the IRTZ (Alatalo et al. 2014b) are able to identify a galaxy as having recently undergone a transformation. Given that post-starburst identification relies on available spectroscopy, being able to use photometry alone to pinpoint transitioning galaxies has the potential to substantially increase the total number of galaxies identified as undergoing this metamorphosis.

The paper is presented as follows. In §2, we describe our post-starburst sample selection and comparison sample. In §3, we describe the post-starburst *WISE* properties and interpret those results. In §4, we summarize our findings. The cosmological parameters $H_0 = 70 \text{ km s}^{-1}$, $\Omega_m = 0.3$ and $\Omega_\Lambda = 0.7$ (Spergel et al. 2007) are used throughout.

2. RESULTS AND ANALYSIS

2.1. Sample Selection

We used the post-starburst galaxy sample defined by Goto (2007) of 564 galaxies from the Sloan Digital Sky Survey Data Release 5 (SDSS DR5; Adelman-McCarthy et al. 2007), selected using the “E+A” criterion of deep Balmer absorption ($\text{EW}(\text{H}\delta) > 5\text{\AA}$) combined with weak nebular ($\text{EW}(\text{H}\alpha) < 3\text{\AA}$, and $\text{EW}(\text{O II}) < 2.5\text{\AA}$) emission. These objects have redshifts ranging between 0.03–0.34. We cross-matched this sample with the *WISE* catalog (Wright et al. 2010) and the SDSS Data Release 9 (DR9; Ahn et al. 2012), using TOPCAT (Taylor 2005). Of the original 564 post-starburst galaxies, 560 have robust ($\text{S/N} > 3$) detections in the W1/3.4 μm , W2/4.6 μm and W3/12 μm bands. 534 objects are detected robustly in u, r, i filters.

In most cases, we used the profile fit (`w*mpro`) value from the *WISE* All-sky catalog for the *WISE* colors. When objects were flagged as extended, we elected to use `w*gmag`, which is the value derived using the 2-Micron All-Sky Survey (2MASS; Skrutskie et al. 2006) profile fit, for the same aperture. The $u-r$ colors are k -corrected using the `calc_kcor`

IDL routine (Chilingarian & Zolotukhin 2012)³.

In order to get a robust sub-selection of objects with near-IR data for a complete spectral energy distribution (SED), we cross-matched the 564 post-starburst galaxies from Goto (2007) with the 2MASS Extended Source Catalog (XSC; Skrutskie et al. 2006), containing the extended source photometries of 1.7 million galaxies⁴. In doing so, we recovered extended source photometries for 190 post-starburst galaxies. Then we cross-matched with the full-photometry catalogs of these samples (containing both SDSS and *WISE* data). Of the 190 post-starbursts, 158 were detected in the *WISE* 3.4, 4.6 and 12 μm bands. Only 53 of the post-starbursts were detected in the *WISE* 22 μm ⁵ band with $\text{S/N} > 3$. For subsequent color plots, we use the 534 E+A galaxies robustly detected in the SDSS $u r i$ bands and *WISE* W1 W2 W3 bands. For subsequent composite spectral energy distribution (SED) plots, we use the 190 XSC E+A galaxies.

For our comparison sample, we use the morphologically classified Galaxy Zoo (Lintott et al. 2008) objects from Schawinski et al. (2014). We also cross-matched these 47,995 Galaxy Zoo objects with the 2MASS XSC, resulting in 38,802 Galaxy Zoo matches. The Galaxy Zoo comparison sample was drawn from Schawinski et al. (2014) and Alatalo et al. (2014b), and a corresponding analysis of the derivation of *WISE* colors can be found therein. Figures 1 & 2 show the optical and *WISE* color distributions of both Galaxy Zoo and the post-starbursts.

2.2. Redshift dependence of the *WISE* colors

Figure 3 shows a significant deviation of the $[3.4]-[4.6]$ *WISE* colors in post-starburst galaxies. Upon closer inspection,

³ <http://kcor.sai.msu.ru/>

⁴ http://www.ipac.caltech.edu/2mass/releases/allsky/doc/sec2_3.html

⁵ The updated filter response function of the *WISE* W4 band places the central wavelength closer to 23 μm (Brown et al. 2014), but we use 22 μm for consistency.

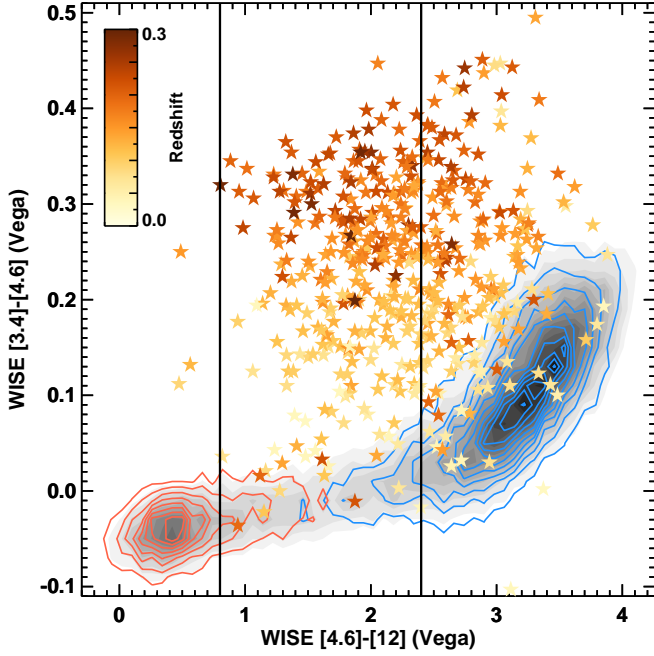


Figure 3. The $[4.6]-[12]$ vs. $[3.4]-[4.6]$ *WISE* colors of post-starbursts (stars) as compared to the early-type (red contours) and late-type (blue contours) galaxies from Schawinski et al. (2014); Alatalo et al. (2014b). The redshift of the post-starbursts are encoded using the color scale on the upper left. A redshift dependence of the $[3.4]-[4.6]$ colors is clear, with the most elevated colors coming from the highest redshift sources.

tion, these colors have a substantial dependence on the redshift of the source, with the most significantly red colors having the highest redshifts. Brown et al. (2014) showed that, given the SEDs of many galaxies go from decreasing to increasing in the mid-IR, accounting for a redshift dependence can be important. Figure 4 shows the $[3.4]-[4.6]$ and $[4.6]-[12]$ colors for the post-starburst sample versus redshift, in both cases showing dependences. This is clear both in the individual post-starburst colors, as well as in the average colors in redshift bins. A slight redshift dependence is also seen in $[4.6]-[12]$ colors, though the trend is smaller than the scatter in each bin. A significant redshift dependence in the $[3.4]-[4.6]$ colors is seen, with a marked increase followed by a flattening at $z \geq 0.2$.

There are many possible causes for this dependence including the effects of aperture bias, Malmquist bias (Malmquist 1925), and redshifting the SED. It is possible that the type of post-starburst galaxy that the (Goto 2007) criterion selected could have changed between the low redshift objects, where the SDSS fiber subtends a smaller fraction of the galaxy and the higher redshift objects, where much more of the galaxy is sampled. It is also possible that the Goto (2007) selection detects brighter, rarer objects at higher redshifts. But given that the mid-IR is the location at which the SED transitions between the Rayleigh-Jeans tail of the stellar light of the galaxy and the hot dust component originating in the circumstellar envelopes of aging stars and shrouded star formation (Silva et al. 1998), it is likely that this has the most dramatic effect on the $[3.4]-[4.6]$ colors. A comprehensive SED fit to these galaxies is required to fully understand how each of these biases might impact our sample, and the constituents to the SED (discussed in §3.2) makes applying accurate k -corrections difficult.

To provide corrections to the $[3.4]-[4.6]$ and $[4.6]-[12]$ colors, we binned the post-starburst galaxies by redshift, every

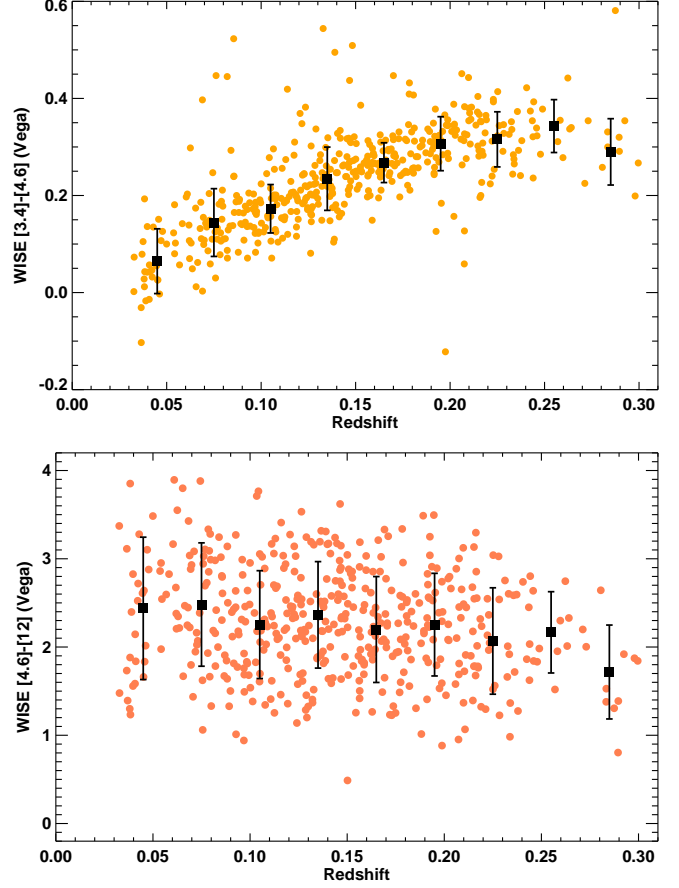


Figure 4. (Top): The $[3.4]-[4.6]$ colors of each of the 560 *WISE*-detected post-starbursts (orange points) versus redshift. The points are then binned in redshift, spaced in bins of $z = 0.03$, ranging from $z = 0.03-0.3$ with $\Delta z = 0.03$. The black squares represent the average $[3.4]-[4.6]$ colors, with error bars representing their standard deviation. A clear redshift dependence is seen in these colors that is more substantial than the scatter in the bins. **(Bottom):** The $[4.6]-[12]$ colors of each of the 560 *WISE*-detected post-starbursts (red points) versus redshift. Black squares represent the average colors in redshift bins with error bars representing the standard deviation. In this case, although there might be a slight trend with redshift, it is well within the (significant) scatter.

$z = 0.03$, from 0.03 to 0.3 with $\Delta z = 0.03$. The average color of each bin was then determined for the colors, shown as the black squares in Fig. 4. The standard deviation of each redshift bin is reflected in the error bars. The Galaxy Zoo sample (Schawinski et al. 2014; Alatalo et al. 2014b) consists of objects with redshifts between $z = 0.02-0.05$. In order to reflect an accurate comparison to Galaxy Zoo, we “correct” the $[3.4]-[4.6]$ and $[4.6]-[12]$ colors of the post-starbursts by normalizing to the $z = 0.03-0.06$ bin. We determine the redshift bin that each individual post-starburst galaxy sits in, then subtract the difference between the average color of that redshift bin from the average color of the $z = 0.03-0.06$ bin. Figures 1 & 2 use *WISE* colors that have been corrected this way.

3. DISCUSSION

3.1. The *WISE* colors of post-starburst galaxies

Figure 1 shows the distribution of the $[4.6]-[12]$ colors of the Galaxy Zoo sample (Schawinski et al. 2014; Alatalo et al. 2014b) separated into the late-type and early-type subsamples with the *WISE* IRTZ overplotted. As was shown in Alatalo et al. (2014b), the Galaxy Zoo samples show a bimodal distribution, with a zone of avoidance between the late-type and early-type populations. The post-starburst sam-

ple is strongly represented within the IRTZ, with $47.6 \pm 2.2\%$ falling within the bounds set in [Alatalo et al. \(2014b\)](#) (compared with $16.1 \pm 0.2\%$ of the Galaxy Zoo sample, $22.7 \pm 0.4\%$ of early-types and $10.5 \pm 0.2\%$ of the late-types), consistent with the hypothesis that the IRTZ is able to pinpoint galaxies that are transitioning. The Mann-Whitney U test (IDL routine `RS_test`) was run to compare each pair of $[4.6] - [12]$ *WISE* color distributions, which confirmed that post-starburst galaxies are a distinct population with a p value $\ll 10^{-5}$ in all cases.

Figure 2 further supports this picture, placing post-starburst galaxies firmly within the transitioning region. Post-starbursts are located primarily in the optical green valley ([Dressler & Gunn 1983](#)) and also appear in the *WISE* IRTZ. The post-starburst population most obviously falls into the transition zone when viewed in $u-r$ vs. *WISE* $[4.6] - [12]$ color space, positioned amongst the tight color correlation between the early-type and late-type populations (Figure 2a). The post-starburst colors confirm that the *WISE* IRTZ traces a transitioning population and can be used as part of a criterion to identify galaxies through their photometry.

Post-starburst galaxies separate themselves into an elevated $[3.4] - [4.6]$ vs. $[4.6] - [12]$ μm *WISE* color space (Fig. 2b; also see Fig. 15 in [Yesuf et al. 2014](#) for the colors of a similar sample). $48 \pm 2\%$ of galaxies fall outside of the 10% contours of the Galaxy Zoo sample, and $91 \pm 1\%$ fall outside the 50% contours of the Galaxy Zoo sample. These colors seem to indicate that post-starbursts do not traverse *WISE* color space through the joint between the early-type and late-types, rather showing signs of elevated $[3.4] - [4.6]$ colors (and intermediate $[4.6] - [12]$ colors) and traversing through a mid-IR “twilight zone.” The zone could be a consequence of the continued presence of ongoing star formation ([Peletier et al. 2012](#); [Hayward et al. 2014](#)), or the presence of an AGN ([van der Wolk 2011](#); [Assef et al. 2013](#); [Mateos et al. 2015](#)).

3.2. The origin of post-starburst *WISE* colors

To further investigate the mid-IR twilight zone, we construct the average SEDs of the post-starbursts, early-types, and late-types. Figure 5 shows the SEDs of each of these subsamples, with the top and bottom of the bar representing the upper and lower quartiles, respectively. The point represents the median value for each band. Early-type galaxies are generally redder than late-type galaxies, and post-starbursts generally fall in between. In the *WISE* bands, the post-starbursts exhibit significantly stronger emission at $[3.4]$ and $[4.6]$ microns as well as a shallower gradient. The $12\mu\text{m}$ flux is generally in between that of the late-type and early-types, with much more overlap with the late-type galaxies.

Figure 6 separates the SEDs of the post-starburst galaxies with (53) or without (108) detected $22\mu\text{m}$ emission. We created a composite SED (with the bars representing the upper and lower quartiles of the distribution, the point representing the median, and the error bars representing the standard deviation of the median) of the $22\mu\text{m}$ detected objects, shown in the first panel of Figure 6. The $12\mu\text{m}$ and $22\mu\text{m}$ SEDs show a leveling off or increasing SED that cannot be reproduced using stars alone ([Bruzual & Charlot 2003](#)). While a compact starburst is capable of creating this rise in the SED, we consider this possibility unlikely. The compact starburst hypothesis assumes that the E+A selection is unable to remove these sources. Given that gas and extreme star formation coalesce into the nucleus of post-merged galaxies ([Mihos & Hernquist](#)

1996; [Bryant & Scoville 1999](#)), it is unlikely that the SDSS spectrum would contain so little $\text{H}\alpha$ emission that it would make it through the E+A cut. Additionally, these buried compact starbursts are inconsistent with the 1.4 GHz radio continuum results in K+A galaxies ([Nielsen et al. 2012](#)).

The $22\mu\text{m}$ emission in post-starbursts not individually detected significantly by *WISE* were stacked to create a composite image. Each $22\mu\text{m}$ thumbnail was downloaded from the ALLWISE⁶ catalog ([Wright et al. 2010](#)). The post-starburst source was placed in the center, and the stacked image was created by taking the average of stacked pixels (4σ outliers in each pixel were clipped to remove contributions from bright stars in individual fields), resulting in a $22\mu\text{m}$ detection from the stack. To extract the photometry of the stacked $22\mu\text{m}$ emission, we used an aperture with radius of $24''$ (i.e., twice the *WISE* $22\mu\text{m}$ resolution). We then subtracted the median emission from the “sky” in an annulus between $35'' < r < 55''$. The resulting photometry (calculated and converted using the *WISE* manual⁷) is: $m = 15.86^{+0.32}_{-0.25}$ in AB magnitudes.

The photometry of each of the 190 XSC post-starburst galaxies was fit using MAGPHYS ([da Cunha et al. 2008](#)), which is described in Appendix A. We isolate the MAGPHYS-derived stellar and hot ($T_{\text{dust}} = 130\text{--}250\text{ K}$) dust luminosity components for each post-starburst, and compare them to early-types, spirals, and AGNs.⁸ We find that $[4.6] - [12]$ color from *WISE* correlates with and is therefore a good proxy for the ratio of the luminosities of the hot dust and stellar emission. This is somewhat expected, as the $4.6\mu\text{m}$ emission primarily traces the stellar blackbody emission and the $12\mu\text{m}$ emission primarily traces hot dust (from either star formation, aged stars, or AGNs).

Figure 7 also shows that the post-starburst have middling luminosity ratios, between early-types and spirals/AGNs. Post-starbursts are expected to be in a transitional state between spirals and early-type galaxies (or possibly rejuvenated early-type galaxies; [Dressler et al. 2013](#); [Abramson et al. 2014](#)), so perhaps their intermediate luminosities are unsurprising. This conclusion, however, assumes though that the hot dust emission has a similar origin to the hot dust emission in spirals (i.e., star formation). Given that the very selection of these galaxies preclude star formation from being significant, it is likely that the hot dust luminosity (and additionally the mid-IR emission from *WISE*) has an alternative heating mechanism. We lay out these possibilities in subsequent sections.

3.2.1. PAHs in post-starbursts

In normal star-forming galaxies, significant emission from photospheres and warm dust and Polycyclic Aromatic Hydrocarbons (PAHs) in the interstellar medium ([Calzetti et al. 2007](#); [Smith et al. 2007](#)) usually overwhelms the mid-IR SED. Thus, in most star-forming galaxies, the *WISE* 12 and $22\mu\text{m}$ bands are detecting active, recent star formation. In extreme starbursts (such as M82), there is a significant compact, hot dust component, leading to a rising SED between 12 and $22\mu\text{m}$ ([Sturm et al. 2000](#); [Beirão et al. 2008](#)). Post-starbursts selected by [Goto \(2007\)](#) removed all objects with significant $\text{H}\alpha$ emission; thus it is unsurprising that their SEDs do not

⁶ <http://wise2.ipac.caltech.edu/docs/release/allwise/>

⁷ http://wise2.ipac.caltech.edu/docs/release/allsky/expsup/sec4_4c.html

⁸ Details on the comparison samples are discussed in Appendix B.

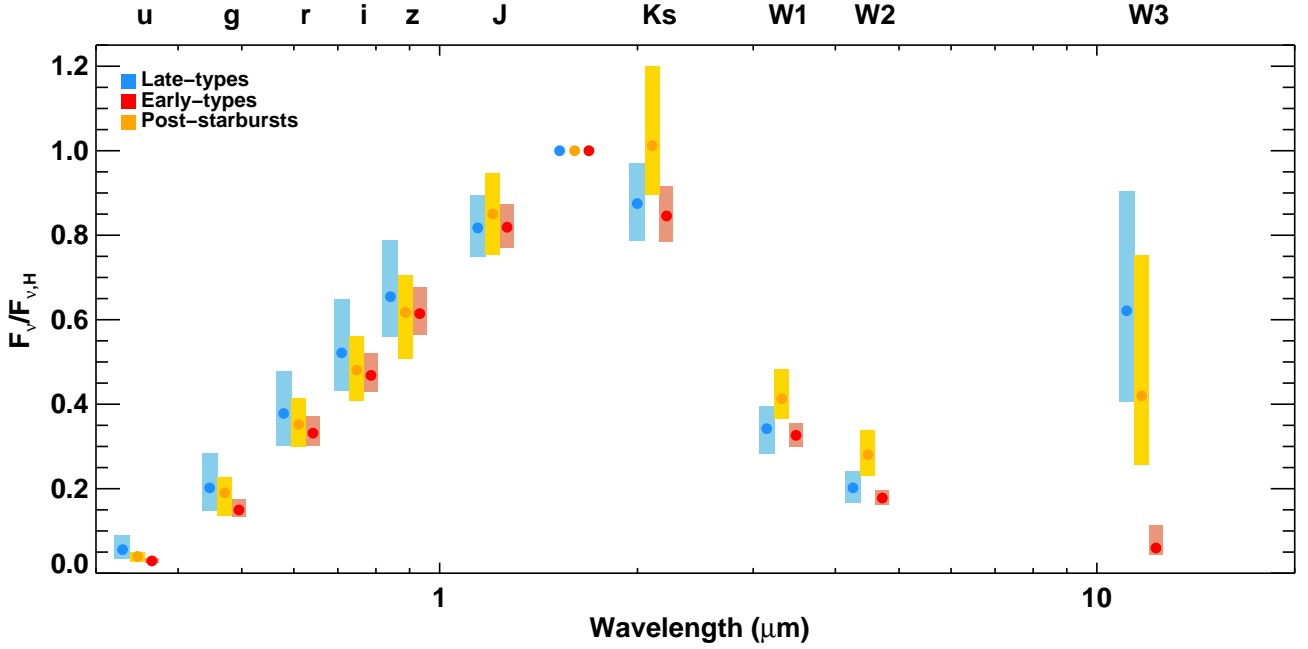


Figure 5. The $ugrizJHK_s$ plus WISE band 1 2 3 **observed frame** spectral energy distributions of each subsample: early-types (red), late-types (blue), and the 158 extended post-starbursts (yellow), normalized to their H -band fluxes. The width of the bar represents the upper and lower quartile, and the point is placed at the median value for each band. Post-starbursts contain colors which are in between early-type and late-type galaxies. Post-starbursts also show significant emission in 3.4 and $4.6\mu\text{m}$, with a shallower gradient. The $12\mu\text{m}$ flux in post-starbursts lies in between the late-type and early-type $12\mu\text{m}$ fluxes, with much more overlap with the late-type galaxies.

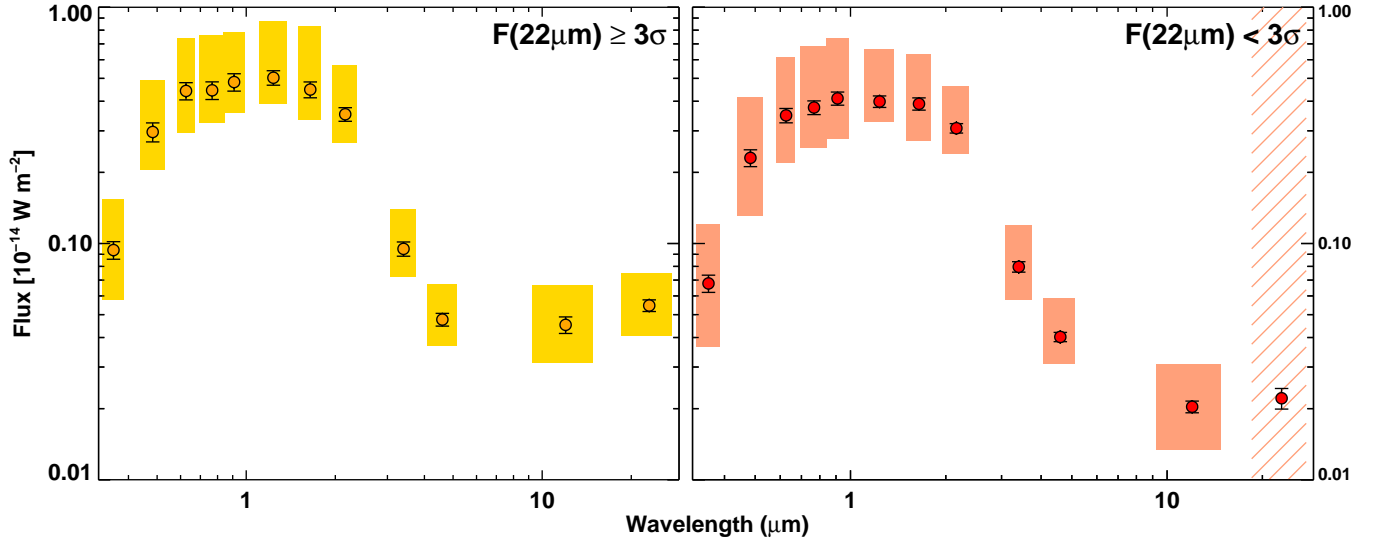


Figure 6. (Left): The composite **observed frame** SED (yellow) of all post-starbursts in our extended catalog detected with $S/N > 3$ ($N = 53$). The width of the boxes represent the bandwidth of each filter, the upper and lower bounds of the boxes represent upper and lower quartiles of the distributions. The points represent the median, and the error bars represent the standard deviation of the median. (Right): The composite SED (red) of all post-starbursts in our extended catalog detected with $S/N < 3$ ($N = 105$), with all features the same as the left panel, except the $22\mu\text{m}$ point, which represents the value from the 4σ -clipped mean-stacked $22\mu\text{m}$ emission. The most significant difference seen in the panels is the strength of the mid-IR (12 and $22\mu\text{m}$) emission, though in both cases, there is an observed flattening in the mid-IR SED.

match those of the star-forming galaxies in Fig. 5, but the enhanced $12\mu\text{m}$ emission (as compared to early-types) is worth discussing further.

By the time the galaxies have quenched and become completely quiescent, the total number of the evolved intermediate age stars has diminished. Therefore, the mid-IR emission in quiescent galaxies likely originates from a diffuse dust component (Temi et al. 2007; Boselli et al. 2010; Ciesla et al. 2014), though usually the dust emission is dwarfed by the stellar emission. PAH emission is detectable in early-type galaxies (Xilouris et al. 2004;

Kaneda et al. 2005, 2008; Bressan et al. 2006; Panuzzo et al. 2007; Bregman et al. 2008) and is significant in K+A galaxies (Roseboom et al. 2009). In both of these cases, the $12\mu\text{m}$ emission is specifically enhanced due to the $11.3\mu\text{m}$ neutral PAH feature, which could explain the significant $12\mu\text{m}$ emission we see in Figure 5. This was argued to be part of the existence of the IRTZ by Alatalo et al. (2014b).

Vega et al. (2010) presented the possibility that the unusual neutral-to-ionized PAH ratios that are observed are not due to accreted gas or an AGN but instead due to the processing of carbonaceous material from the circumstellar envelopes

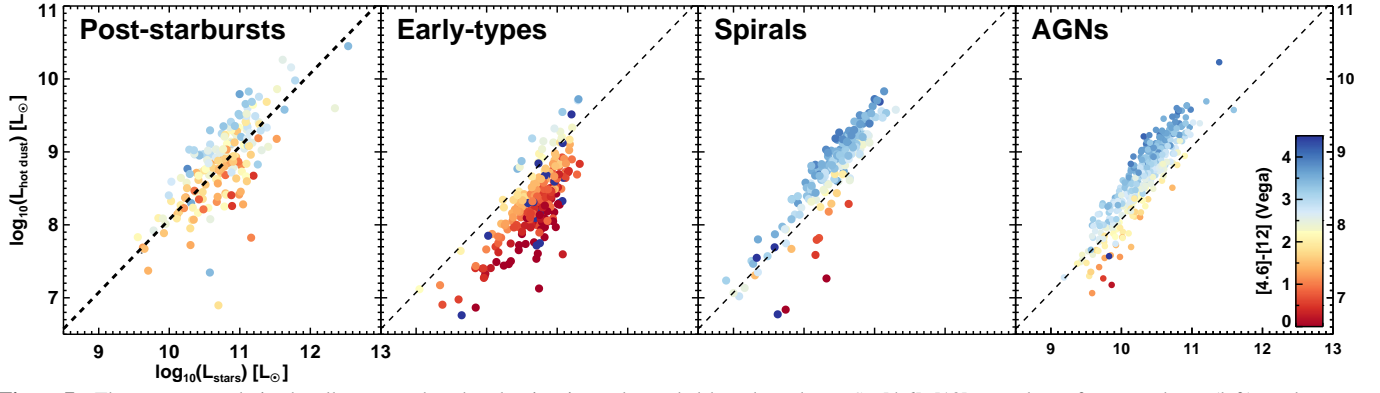


Figure 7. The MAGPHYS-derived stellar versus hot dust luminosity, color-coded based on the *WISE* [4.6]–[12] μm colors of post-starburst (left), early-type galaxies (middle left), spirals (middle right), and AGNs (right). The stellar luminosity range is the same in all panels. The dashed black line corresponds to the mean relationship between the stellar and hot dust luminosities for the post-starbursts in all panels. The *WISE* [4.6]–[12] μm colors are correlated with the relative strength of the hot dust (compared to stellar) luminosities. Early-type galaxies are the most stellar luminosity-dominant, and both spirals and AGNs have larger hot dust (compared to stellar) luminosities, though it is likely that the hot dust emission originates from a different source for each. Post-starbursts have hot dust-to-stellar luminosities that are between the early-type and spiral or AGN values.

of Thermally Pulsating Asymptotic Giant Branch (TP-AGB) stars combined with slow shocks. These combination of these two processes may be able to create amorphous carbon and destroy the smaller PAHs (that create the shorter wavelength ionized PAH bands), leading to the enhanced $11.3\mu\text{m}$ neutral emission. Thus, it is possible that $11.3\mu\text{m}$ PAH emission (a potential source for the enhanced $12\mu\text{m}$ emission) could originate from TP-AGB stars.

3.2.2. AGB stars in post-starbursts

Figure 8 presents the [4.6]–[12] vs. [12]–[22] *WISE* colors for Oxygen-rich asymptotic giant branch (AGB) stars (Suh & Kwon 2011), Stripe 82⁹ “strong” AGNs¹⁰ (blue points; Glikman et al., in prep), $22\mu\text{m}$ non-detected (dark orange triangles), and $22\mu\text{m}$ -detected post-starbursts (yellow stars). For many of the post-starbursts (both $22\mu\text{m}$ detected and non-detected), the [4.6]–[12] colors are consistent with oxygen-rich AGB stars, whose contributions to the optical spectra peak during the post-starburst phase of a galaxy (Yan et al. 2006), and are inconsistent with the normal star-forming population (as is seen in the [4.6]–[12] color comparison in Fig. 2).

Post-starburst galaxies are an ideal population to study mid-IR emission from the AGB population, given that their star formation has been quenched and no longer contributes, and the intermediate age stars are still abundant. Emission from circumstellar dust shells originating in TP-AGB stars tend to peak in the mid-IR (Piovan et al. 2003; Maraston 2005; Kelson & Holden 2010; Chisari & Kelson 2012). A 2 Gyr old AGB component leads to a slightly shallower slope in the mid-IR portion of the SED, which is observed in the post-starburst composite SED in Figure 5.

Previous studies of the TP-AGB and post-AGB contributions to post-starbursts have been contradictory, with optical spectra suggestive of their contribution (Yan et al. 2006) but IR spectra (Zibetti et al. 2013) and SED studies inconsistent with a dominant AGB component (Kriek et al. 2010; Melnick & De Propriis 2013). In the cases of the contrasting studies, many used models that required a “heavy” AGB contribution that did not include circumstellar dust (Maraston 2005) and did not fit the SED out to the mid-IR. When mid-IR data are included, and the AGB model is modified to include

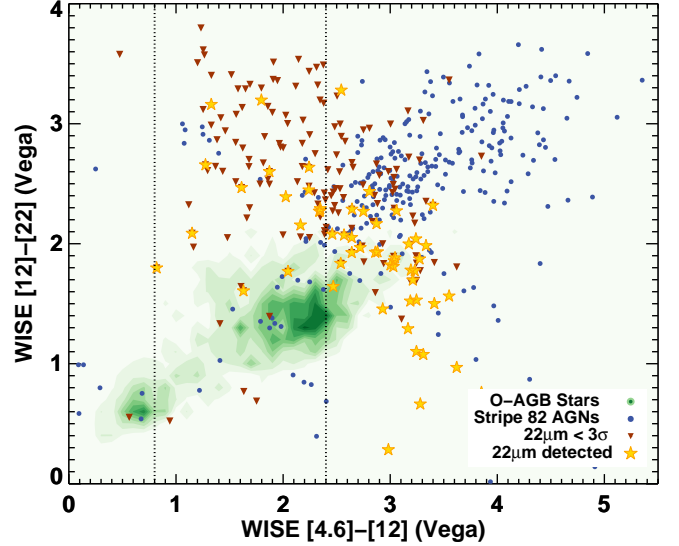


Figure 8. The [4.6]–[12] vs. [12]–[22] *WISE* colors for Oxygen-rich AGB stars (green colorscale; Suh & Kwon 2011), Stripe 82 “strong” AGNs (blue points; Glikman et al., in prep), $22\mu\text{m}$ non-detected (dark triangles) and $22\mu\text{m}$ -detected post-starbursts (yellow stars) from the extended source sample of 158. The IRTZ is represented by black dotted lines. As was shown in Figures 1 & 2, post-starbursts fall in the infrared transition zone. Many post-starbursts exhibit [12]–[22] colors consistent with AGNs.

circumstellar dust, TP-AGB and post-AGB models more consistently match the SEDs (Maraston et al. 2013). The [4.6]–[12] colors from Fig. 8 seem to indicate that these stars could contribute to the mid-IR SED of post-starbursts, but the data are inconclusive. Thus, it is not clear what impact TP-AGB and post-AGB stars have on the integrated light of post-starburst galaxies; it will require further study to disentangle from other contributors to the $12\mu\text{m}$ portion of a galaxy’s SED.

3.2.3. AGNs in post-starbursts

The *WISE* [3.4]–[4.6] vs. [4.6]–[12] colors of post-starburst galaxies shown in Figure 2b suggest that the transition in infrared color space of these objects is not a simple pathway in color space across the boundary that separates the early-type and late-type galaxy distributions. A robust exploration of the physical processes taking place in the quenching galaxies, and how those manifest in their integrated properties, can shed light on the way in which post-starburst galaxies undergo

⁹ <http://classic.sdss.org/legacy/stripe82.html>

¹⁰ AGNs that are brighter than their hosts’ starlight

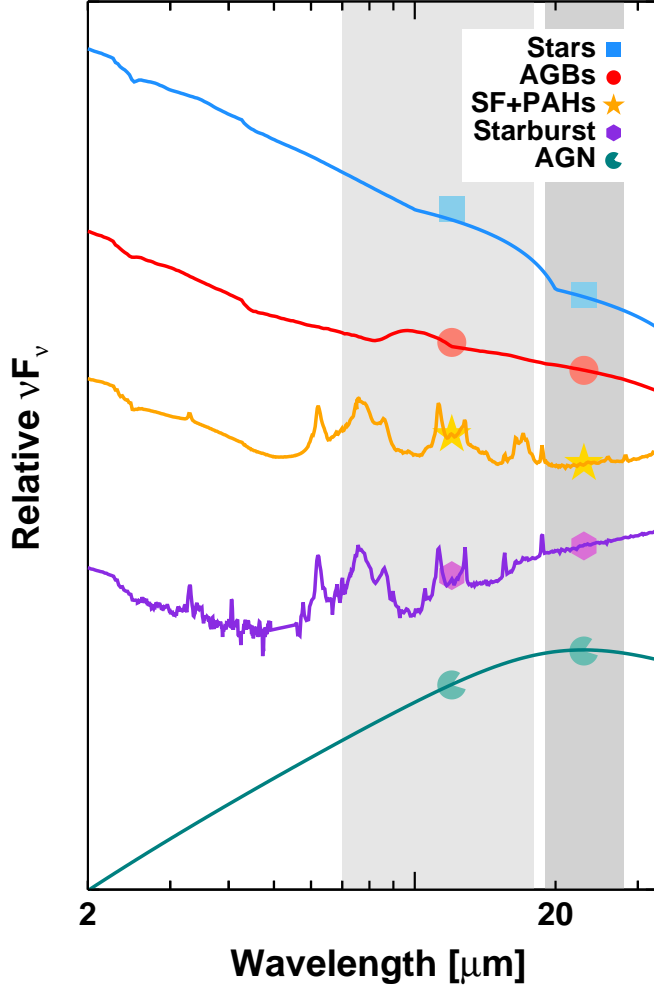


Figure 9. The 2–30 μm region of various models of different objects, including a pure stellar population (blue; [Bruzual & Charlot 2003](#)), AGB stars (red; [Piovan et al. 2003](#)), star-forming galaxies including PAH emission (orange; [Brown et al. 2014](#)), starbursts (purple; [Brown et al. 2014](#)), and an AGN (teal; [Sajina et al. 2012](#)). The grayed regions represent the bandwidth of the *WISE* 12 μm and 22 μm filters. The blocks show the mean value of each model across the *WISE* bands. In all cases except for that of the starburst and AGN, it appears that the SEDs decrease with increasing wavelength.

their metamorphosis.

Post-starburst galaxies are thought to be the final stage of a transitioning galaxy. Evidence exists that there is a delay between star formation quenching and the onset of AGN activity ([Canalizo & Stockton 2001](#); [Schawinski et al. 2007](#); [Kaviraj et al. 2015](#); [Matsuoka et al. 2015](#); [Bitsakis et al. 2016](#)); thus, we might expect post-starburst galaxies to disproportionately host AGNs, assuming that they are just post-transition. The distribution of post-starburst *WISE* colors in fact show similarities to the Seyfert population discussed in [Alatalo et al. \(2014b\)](#). Could this be a sign that the *WISE* colors of post-starburst galaxies originate from a buried AGN component?

Many studies into post-starbursts have aimed to confirm the presence of AGNs in these systems. [Brown et al. \(2009\)](#) observed a slight enhancement in X-rays in a sample of K+A galaxies in the NOAO Deep Wide-field Survey, though not to a significance to be definitively from AGN emission. [Shin et al. \(2011\)](#) cross-identify 1.4 GHz FIRST ([Becker et al. 1995](#)) sources with the [Goto \(2007\)](#) E+A sample, but detections are ambiguous (most sources unresolved and lacking

clear radio jets). [Nielsen et al. \(2012\)](#) cross-referenced K+A galaxies with FIRST ([Becker et al. 1995](#)), and noted enhanced radio emission in some of them, which could be attributed to either AGN activity or remnant star formation. Though all of these studies could be pointing to low-luminosity AGNs being present, none are definitive. [Meusinger et al. \(2017\)](#) studied a large sample of E+A galaxies, finding a slightly elevated number of luminous ($> 10^{23}$ W) 1.4 GHz continuum sources and enhanced fraction of mid-IR *WISE* selected ([Assef et al. 2013](#)) AGNs, and confirmed the rising mid-IR SED discussed by [Melnick & De Propriis \(2013\)](#), but concluded while E+A galaxies do not host strong AGNs, they may contain obscured and/or low-luminosity AGNs or require significant emission from post-AGB stars (as discussed in §3.2.2).

The right panel of Figure 6 shows the composite SED created from the 105 *WISE* 22 μm non-detected objects, with quartiles and medians from data points up to 12 μm consistent with the right panel. In these objects, there is a more significant drop between the 4.6 μm data point and the 12 μm , but there is still observed flattening in the mid-IR.

The 22 μm emission can also be produced by remnant hot dust emission from the recently quenched episode of star formation, which has been known to cause the overestimation of star formation in these types of sources ([Hayward et al. 2014](#); [Utomo et al. 2014](#)). Sources that show these overestimates often show a decrease between the 12 and 22 μm bands, which is not the behavior that we observe in our sample in Figure 6. Alternative processes able to create a rising mid-IR SED at wavelengths shorter than 10 μm and provide sufficient emission to balance the stellar light from the galaxy are starbursts or AGNs. Starbursts have been ruled out by the weak nebular emission in the post-starburst systems ([Goto 2007](#)), especially since the majority of post-merger star formation activity is expected to occur in the nucleus ([Mihos & Hernquist 1996](#)), at the position of the SDSS spectral fiber. Figure 9 shows the 2–30 μm ranges of five phenomena that contribute to the mid-IR SED including stellar emission ([Bruzual & Charlot 2003](#)), AGB stars ([Piovan et al. 2003](#)), star formation and PAH emission (NGC 3521; [Brown et al. 2014](#)), a starburst galaxy (Mrk 33; [Brown et al. 2014](#)), hot dust from an AGN ([Sajina et al. 2012](#)). Both the starburst and AGN hot dust templates exhibit rising mid-IR emission, but it is improbable that the majority of post-starburst galaxies contain buried H II regions from prolific star formation. This leaves open the possibility that the remnant hot dust emission seen is being heated by low-luminosity AGNs.

Assuming that 100% of the derived hot dust luminosity in the post-starburst galaxies originates from an AGN, we estimated the Eddington ratios for each 2MASS XSC post-starburst, which is detailed in Appendix C. The resultant Eddington ratios range between 10^{-2} – 10^{-4} , with a peak around 10^{-3} . This firmly places these possible post-starburst AGNs into the low-luminosity regime. These Eddington ratios are also strict upper limits, as it is unlikely that in all sources, 100% of the hot dust luminosity is due to an AGN (since intermediate-aged stars also produce hot dust emission in post-starbursts as well).

To determine the X-ray properties of the 2MASS XSC post-starbursts, we cross-matched them with the *Swift* 70-month BAT All-sky Hard X-ray Survey ([Baumgartner et al. 2013](#)) but were unable to match any objects. Given the low Eddington ratio upper limits that the post-starburst 2MASS XSC samples, this is unsurprising, (the flux limit of the *Swift* BAT catalog is 1.03×10^{11} erg s $^{-1}$ cm $^{-2}$, thus finds mainly high

luminosity AGNs).

We also cross-matched the 2MASS XSC post-starbursts with the *Chandra* archive. Four were targeted by *Chandra* (ObsIDs 10270–10273; PI Zabludoff), and all four have weak-to-moderate detections above background fluctuations in a $2''$ aperture at the center of the galaxy. We use WEBPIMMS to calculate the associated observed 2–10 keV luminosities ranging between 10^{40} to 6×10^{40} , assuming a power law with $\Gamma=1.8$. The corresponding Eddington ratios (assuming $L_X \approx 1/16 L_{\text{bol}}$; Ho 2008) range between 10^{-5} – $10^{-4.5}$.¹¹ Another four were serendipitously in the fields of view of other *Chandra* observations of comparable exposure times but were not detected to significance above the background. That X-rays were detected coincident with the nuclei of many of the post-starbursts that were observed does provide further evidence that post-starbursts may contain an AGN phase, but given the small number statistics that still exist for these objects, is not conclusive.

Our estimate of possible Eddington ratios of the post-starbursts, derived from the hot dust luminosity, combined with the X-ray results seems to indicate that the presence of these low-luminosity AGNs in post-starbursts is entirely feasible given the estimated energetics. These results also support the conclusion of De Propriis & Melnick (2014), that AGNs in post-starburst galaxies are not radiatively significant. The $H\alpha$ fluxes necessary to pass the Goto (2007) criterion seems to rule out radiatively significant AGNs, and in the case of the 2MASS XSC post-starbursts, do not likely represent Eddington ratios above $\sim 10^{-3}$. Burying the AGN under a reservoir of optically thick gas is able to significantly impact the $H\alpha$ emission that can be observed, while the mid-IR AGN light is able to escape.

The E+A criterion selects against the presence of strong AGNs, quasars, and shocked systems (as these objects all emit $H\alpha$ or [O II] emission). Thus the possibility of AGNs being the source for the mid-IR colors is not a certainty. But new studies have opened up the possibility that there may be buried low-luminosity AGNs in post-starburst galaxies. Recently, significant molecular gas reservoirs have been discovered in post-starburst galaxies (French et al. 2015; Rowlands et al. 2015). These CO-rich post-starbursts also exhibit excess $22\mu\text{m}$ emission compared to their CO(1–0) emission, diverging from the relation set by the star-forming galaxies (Alatalo et al. 2016b). Additionally, the optical spectra of post-starbursts (despite having weak nebular lines) have LINER-like line emission, consistent with what is observed in low-luminosity AGNs (Yan et al. 2006; Yang et al. 2006). LINER emission also often originates from other sources, such as aged stellar populations (Yan et al. 2006; Sarzi et al. 2010) and shocks (Allen et al. 2008; Rich et al. 2011; Alatalo et al. 2016a), so this LINER emission is also not confirmatory of AGNs. The post-starburst composite SEDs and *WISE* colors support the possibility that many post-starbursts contain buried AGNs, which is not contradicted by the ionized gas line emission properties, and may even be supported by the presence of gas (and therefore an obscuring column).

A broad statistical analysis on emission line galaxies from SDSS showed that the AGN fraction in disk-dominated star-forming galaxies is significantly underestimated (Trump et al.

2015), their signals being overwhelmed by the ionized gas signatures associated with star formation. Bitsakis et al. (2015, 2016) note that in compact group galaxies (a known rapidly evolving population), once star formation started shutting down, the fraction of AGN-hosting galaxies increases even as the AGN luminosity decreases. These trends suggest either that weak AGN were always present in the nuclei of these galaxies but was being out-shined by star formation or that weak AGN activity begins during the phase of star formation quenching; it is unclear whether this result is universal. Our results fuel further discussion about whether the quenching of star formation reduces the mid-IR signal that overwhelmed the weak AGN (Trump et al. 2015) or whether AGN fueling is part of the transition process (Hopkins et al. 2008). Studying whether the mid-IR slope changes as a function of the stellar population age in post-starbursts may be able to discriminate between these two scenarios, but is beyond the scope of this paper.

3.3. Toward a comprehensive selection of transitioning galaxies

Selecting transitioning galaxies has long been a challenging endeavor. Optical colors can be ambiguous (Schawinski et al. 2014); ultraviolet colors tend to be ultra-sensitive to star formation activity down to 1% mass fractions (Kaviraj et al. 2007a,b; Choi et al. 2009), creating a set of “frosted” early-type galaxy interlopers. Robust spectral classification can be expensive, requiring high signal-to-noise spectra to detect absorption against the stellar continuum, placing the detection and cataloging high-redshift quenched galaxies out of reach. Wild et al. (2014) showed that “super-colors” could be used to identify post-starburst-like galaxies in the redshift range $0.9 < z < 1.2$, but this method has not been useful at lower redshift, due to its dependence on the ultraviolet portion of the SED.

Our new work opens yet another door to finding quenching galaxies, using the mid-IR colors. An independent investigation by Ko et al. (2016) found that stacked spectra of mid-IR excess galaxies (defined using [3.4]–[12] *WISE* colors) showed signs of an intermediate stellar population. Post-starbursts, the bonafide transitioning population, sit in a distinct phase space in the *WISE* [3.4]–[4.6] vs. [4.6]–[12] colors, which, in the era of the *James Webb Space Telescope*, we will be able to observe up to $z \approx 1$.

Our work has also introduced a new challenge to how we identify quenching galaxies. Given that some post-starburst sources show signs of the presence of an AGN, it is likely that we are missing a significant population of quenching galaxies simply because we are removing all galaxies with significant emission in either $H\alpha$ or [O II], which an AGN will excite. That AGNs are present in E+A galaxies *whose selection criteria directly select against them* tells us that the AGNs are a crucial ingredient to study when trying to understand the nature of quenching galaxies, and should not be excluded when attempting to create a complete picture of galaxy metamorphosis, even at $z=0$ (and especially at high redshift).

4. SUMMARY

We have analyzed the mid-IR properties of a selection of post-starburst galaxies selected through the “E+A” criterion by Goto (2007) from SDSS DR7 (Abazajian et al. 2009). Of the original 564 post-starbursts, we were able to analyze the colors of 534 objects with robust detections from both SDSS

¹¹ One of the four sources (that with the highest X-ray flux) did not have sufficiently accurate spectroscopy to measure σ_* , thus we were unable to derive an accurate Eddington ratio.

and *WISE* 3.4, 4.6, and $12\mu\text{m}$. We further investigated post-starbursts detected in the 2MASS XSC, totaling 190 objects, of which 158 have robust $3.4\mu\text{m}$, $4.6\mu\text{m}$ and $12\mu\text{m}$ detections. 53 of the 2MASS XSC post-starbursts are robustly ($S/N > 3$) detected in the *WISE* $22\mu\text{m}$ band. Using these samples, we came to the following conclusions.

The 534 post-starburst galaxies studied have transitioning $u-r$ and $[4.6]-[12]$ colors, falling within the infrared transition zone discussed by Alatalo et al. (2014b).

After correcting for redshift effects, the $[3.4]-[4.6]$ vs. $[4.6]-[12]$ colors of post-starburst galaxies stand out from the colors of both early-type and late-type galaxies, inhabiting the mid-IR twilight zone. This result shows that galaxies do not transition directly across the mid-IR color gap between the early-type and late-type population, requiring an additional source of mid-IR emission.

The SED of post-starburst galaxies requires the inclusion of either strong neutral ($11.3\mu\text{m}$) PAH emission or a TP-AGB component (with circumstellar dust) to fit the $3-12\mu\text{m}$ data. A TP-AGB component would also be consistent with the findings of Yan et al. (2006), which required this component to explain the ionized gas emission seen in post-starbursts.

We used MAGPHYS to fit the SEDs of the XSC post-starbursts, extracting the stellar and hot dust luminosities. We find that post-starbursts have intermediate hot dust luminosities (compared to the stellar), and that the $[4.6]-[12]\mu\text{m}$ *WISE* colors are a good proxy for the ratio between L_\star and $L_{\text{hot dust}}$.

The composite SEDs of our observed post-starbursts (with $22\mu\text{m}$ emission detected with $S/N > 3$) suggest that an AGN component is needed to account for the hot dust detected in the $22\mu\text{m}$ *WISE* band, but we cannot rule out other possibilities. Stacking the $22\mu\text{m}$ emission in non-detected post-starbursts was also consistent with the need for a hot dust component to explain a flat mid-IR composite SED. The upper limit to the Eddington ratios inferred from the hot dust luminosity range between $10^{-4}-10^{-2}$, with an average of 10^{-3} . This suggests that while AGNs might be present, they are low-luminosity and not radiatively dominant in the system.

Identifying galaxies that are transitioning requires a multi-wavelength approach, and a closer look at the mid-IR has revealed new and exciting results. *WISE* colors suggest a path forward to photometrically identifying galaxies that are transitioning. SEDs of post-starbursts that include $22\mu\text{m}$ emission suggest the presence of AGNs may be important for some of them, despite their ionized gas selection biasing against the presence of AGNs. We suggest that neglecting to allow for the presence of AGNs when selecting transitioning galaxies may be presenting a biased picture of how metamorphosis takes place.

K.A. thanks R. Peletier for useful discussions as this manuscript was being prepared, as well as the anonymous referee for excellent suggestions that strengthened the manuscript. Support for K.A. is provided by NASA through Hubble Fellowship grant #HST-HF2-51352.001 awarded by the Space Telescope Science Institute, which is operated by the Association of Universities for Research in Astronomy, Inc., for NASA, under contract NAS5-26555. P.N.A. is partially supported by funding through *Herschel*, a European Space Agency Cornerstone Mission with significant participation by NASA, through an award issued by JPL/Caltech. T.B. would like to acknowledge support from

the CONACyT Research Fellowships program. S.L.C. was supported by ALMA-CONICYT program 31110020. J. F.-B. acknowledges support from grant AYA2016-77237-C3-1-P from the Spanish Ministry of Economy and Competitiveness (MINECO). L.L. acknowledges support for this work provided by NASA through an award issued by JPL/Caltech. K.N. acknowledges support from NASA through the *Spitzer* Space Telescope. L.J.K. and A.M.M. acknowledge the support of the Australian Research Council (ARC) through Discovery project DP130103925. L.C. received funding from the European Union Seventh Framework Programme (FP7/2007-2013) under grant agreement n 312725. Support for A.M.M. is provided by NASA through Hubble Fellowship grant #HST-HF2-51377 awarded by the Space Telescope Science Institute, which is operated by the Association of Universities for Research in Astronomy, Inc., for NASA, under contract NAS5-26555.

This publication makes use of data products from the Wide-field Infrared Survey Explorer, which is a joint project of the University of California, Los Angeles, and the Jet Propulsion Laboratory/California Institute of Technology, funded by the National Aeronautics and Space Administration. The National Radio Astronomy Observatory is a facility of the National Science Foundation operated under cooperative agreement by Associated Universities, Inc.

Facilities: Sloan, WISE

REFERENCES

- Aalto S., Muller S., Sakamoto K., et al., 2012, *A&A*, **546**, A68
Aalto S., Costagliola F., Muller S., et al., 2016, *A&A*, **590**, A73
Abazajian K. N., Adelman-McCarthy J. K., the SDSS Collaboration et al., 2009, *ApJS*, **182**, 543
Abramson L. E., Kelson D. D., Dressler A., et al., 2014, *ApJ*, **785**, L36
Adelman-McCarthy J. K., Agüeros M. A., Allam S. S., et al., 2007, *ApJS*, **172**, 634
Ahn C. P., Alexandroff R., the SDSS Collaboration et al., 2012, *ApJS*, **203**, 21
Alatalo K., 2015, *ApJ*, **801**, L17
Alatalo K., Blitz L., Young L. M., et al., 2011, *ApJ*, **735**, 88
Alatalo K., Nyland K., Graves G., et al., 2014a, *ApJ*, **780**, 186
Alatalo K., Cales S. L., Appleton P. N., et al., 2014b, *ApJ*, **794**, L13
Alatalo K., Lacy M., Lanz L., et al., 2015a, *ApJ*, **798**, 31
Alatalo K., Appleton P. N., Lisenfeld U., et al., 2015b, *ApJ*, **812**, 117
Alatalo K., Cales S. L., Rich J. A., et al., 2016a, *ApJS*, **224**, 38
Alatalo K., Lisenfeld U., Lanz L., et al., 2016b, *ApJ*, **827**, 106
Allen M. G., Groves B. A., Dopita M. A., et al., 2008, *ApJS*, **178**, 20
Appleton P. N., Guillard P., Boulanger F., et al., 2013, *ApJ*, **777**, 66
Assef R. J., Stern D., Kochanek C. S., et al., 2013, *ApJ*, **772**, 26
Baade W., 1958, *Ricerche Astronomiche*, **5**, 3
Baldry I. K., Glazebrook K., Brinkmann J., et al., 2004, *ApJ*, **600**, 681
Baumgartner W. H., Tueller J., Markwardt C. B., et al., 2013, *ApJS*, **207**, 19
Becker R. H., White R. L., Helfand D. J., 1995, *ApJ*, **450**, 559
Beirão P., Brandl B. R., Appleton P. N., et al., 2008, *ApJ*, **676**, 304
Bekki K., 1998, *ApJ*, **502**, L133
Bekki K., Couch W. J., Shioya Y., 2002, *ApJ*, **577**, 651
Bertin E., Arnouts S., 1996, *A&AS*, **117**, 393
Bitsakis T., Charmandaris V., da Cunha E., et al., 2011, *A&A*, **533**, A142
Bitsakis T., Charmandaris V., Appleton P. N., et al., 2014, *A&A*, **565**, A25
Bitsakis T., Dultzin D., Ciesla L., et al., 2015, *MNRAS*, **450**, 3114
Bitsakis T., Dultzin D., Ciesla L., et al., 2016, *MNRAS*, **459**, 957
Blanton M. R., Moustakas J., 2009, *ARA&A*, **47**, 159
Borthakur S., Yun M. S., Verdes-Montenegro L., 2010, *ApJ*, **710**, 385
Boselli A., Ciesla L., Buat V., et al., 2010, *A&A*, **518**, L61
Bregman J. D., Bregman J. N., Temi P., 2008, in Chary R.-R., Teplitz H. I., Sheth K., eds, *Astronomical Society of the Pacific Conference Series Vol. 381, Infrared Diagnostics of Galaxy Evolution*. p. 34
Bressan A., Panuzzo P., Buson L., et al., 2006, *ApJ*, **639**, L55
Brown M. J. I., Moustakas J., Caldwell N., et al., 2009, *ApJ*, **703**, 150
Brown M. J. I., Jarrett T. H., Cluver M. E., 2014, *PASA*, **31**, HASH
Bruzual G., Charlot S., 2003, *MNRAS*, **344**, 1000
Bryant P. M., Scoville N. Z., 1999, *AJ*, **117**, 2632

- Cales S. L., Brotherton M. S., 2015, *MNRAS*, **449**, 2374
- Cales S. L., Brotherton M. S., Shang Z., et al., 2011, *ApJ*, **741**, 106
- Cales S. L., Brotherton M. S., Shang Z., et al., 2013, *ApJ*, **762**, 90
- Calzetti D., Kennicutt R. C., Engelbracht C. W., et al., 2007, *ApJ*, **666**, 870
- Canalizo G., Stockton A., 2000, *AJ*, **120**, 1750
- Canalizo G., Stockton A., 2001, *ApJ*, **555**, 719
- Canalizo G., Stockton A., 2013, *ApJ*, **772**, 132
- Chabrier G., 2003, *PASP*, **115**, 763
- Charlot S., Fall S. M., 2000, *ApJ*, **539**, 718
- Chilingarian I. V., Zolotukhin I. Y., 2012, *MNRAS*, **419**, 1727
- Chisari N. E., Kelson D. D., 2012, *ApJ*, **753**, 94
- Choi Y., Goto T., Yoon S.-J., 2009, *MNRAS*, **395**, 637
- Cicone C., Feruglio C., Maiolino R., et al., 2012, *A&A*, **543**, A99
- Cicone C., Maiolino R., Sturm E., et al., 2014, *A&A*, **562**, A21
- Ciesla L., Boquien M., Boselli A., et al., 2014, *A&A*, **565**, A128
- Costagliola F., Herrero-Illana R., Lohfink A., et al., 2016, *A&A*, **594**, A114
- Croton D. J., Springel V., White S. D. M., et al., 2006, *MNRAS*, **365**, 11
- Davis T. A., Krajnović D., McDermid R. M., et al., 2012, *MNRAS*, **426**, 1574
- Davis T. A., Young L. M., Crocker A. F., et al., 2014, *MNRAS*, **444**, 3427
- De Propriis R., Melnick J., 2014, *MNRAS*, **439**, 2837
- Di Matteo T., Springel V., Hernquist L., 2005, *Nature*, **433**, 604
- Dressler A., Gunn J. E., 1983, *ApJ*, **270**, 7
- Dressler A., Oemler Jr. A., Poggianti B. M., et al., 2013, *ApJ*, **770**, 62
- Eliche-Moral M. C., González-García A. C., Aguerri J. A. L., et al., 2012, *A&A*, **547**, A48
- Feruglio C., Maiolino R., Piconcelli E., et al., 2010, *A&A*, **518**, L155
- Fischer J., Sturm E., González-Alfonso E., et al., 2010, *A&A*, **518**, L41
- French K. D., Yang Y., Zabludoff A., et al., 2015, *ApJ*, **801**, 1
- Goto T., 2005, *MNRAS*, **357**, 937
- Goto T., 2007, *MNRAS*, **377**, 1222
- Guillard P., Boulanger F., Lehnert M. D., et al., 2015, *A&A*, **574**, A32
- Hayward C. C., Lanz L., Ashby M. L. N., et al., 2014, *MNRAS*, **445**, 1598
- Hickson P., Mendes de Oliveira C., Huchra J. P., Palumbo G. G., 1992, *ApJ*, **399**, 353
- Ho L. C., 2008, *ARA&A*, **46**, 475
- Holmberg E., 1958, *Meddelanden fran Lunds Astronomiska Observatorium Serie II*, **136**, 1
- Hopkins P. F., Hernquist L., Cox T. J., et al., 2006, *ApJS*, **163**, 1
- Hopkins P. F., Hernquist L., Cox T. J., Kereš D., 2008, *ApJS*, **175**, 356
- Hubble E. P., 1926, *ApJ*, **64**, 321
- Johnson K. E., Hibbard J. E., Gallagher S. C., et al., 2007, *AJ*, **134**, 1522
- Kaneda H., Onaka T., Sakon I., 2005, *ApJ*, **632**, L83
- Kaneda H., Onaka T., Sakon I., et al., 2008, *ApJ*, **684**, 270
- Kannappan S. J., Stark D. V., Eckert K. D., et al., 2013, *ApJ*, **777**, 42
- Kaviraj S., Schawinski K., Devriendt J. E. G., et al., 2007a, *ApJS*, **173**, 619
- Kaviraj S., Kirkby L. A., Silk J., Sarzi M., 2007b, *MNRAS*, **382**, 960
- Kaviraj S., Shabala S. S., Deller A. T., Middelberg E., 2015, *MNRAS*, **452**, 774
- Kelson D. D., Holden B. P., 2010, *ApJ*, **713**, L28
- Ko J., Hwang H. S., Lee J. C., Sohn Y.-J., 2013, *ApJ*, **767**, 90
- Ko J., Chung H., Hwang H. S., Lee J. C., 2016, *ApJ*, **820**, 132
- Kormendy J., Ho L. C., 2013, *ARA&A*, **51**, 511
- Kriek M., Labbé I., Conroy C., et al., 2010, *ApJ*, **722**, L64
- Lang D., Hogg D. W., Schlegel D. J., 2016, *AJ*, **151**, 36
- Lanz L., Ogle P. M., Evans D., et al., 2015, *ApJ*, **801**, 17
- Lanz L., Ogle P. M., Alatalo K., Appleton P. N., 2016, *ApJ*, **826**, 29
- Lintott C. J., Schawinski K., Slosar A., et al., 2008, *MNRAS*, **389**, 1179
- Lintott C., Schawinski K., Bamford S., et al., 2011, *MNRAS*, **410**, 166
- Lisenfeld U., Appleton P. N., Cluver M. E., et al., 2014, *A&A*, **570**, A24
- Lusso E., Hennawi J. F., Comastri A., et al., 2013, *ApJ*, **777**, 86
- Malmquist K. G., 1925, *Meddelanden fran Lunds Astronomiska Observatorium Serie I*, **106**, 1
- Maraston C., 2005, *MNRAS*, **362**, 799
- Maraston C., Pforr J., Henriques B. M., et al., 2013, *MNRAS*, **435**, 2764
- Martig M., Bournaud F., Teyssier R., Dekel A., 2009, *ApJ*, **707**, 250
- Martig M., Crocker A. F., Bournaud F., et al., 2013, *MNRAS*, **432**, 1914
- Martinez-Badenes V., Lisenfeld U., Espada D., et al., 2012, *A&A*, **540**, A96
- Mateos S., Carrera F. J., Alonso-Herrero A., et al., 2015, *MNRAS*, **449**, 1422
- Matsuoka Y., Strauss M. A., Shen Y., et al., 2015, *ApJ*, **811**, 91
- Melnick J., De Propriis R., 2013, *MNRAS*, **431**, 2034
- Meusinger H., Brünecke J., Schallbach P., in der Au A., 2017, *A&A*, **597**, A134
- Mihos J. C., 1995, *ApJ*, **438**, L75
- Mihos J. C., Hernquist L., 1996, *ApJ*, **464**, 641
- Moore B., Katz N., Lake G., Dressler A., Oemler A., 1996, *Nature*, **379**, 613
- Morrissey P., Conrow T., Barlow T. A., et al., 2007, *ApJS*, **173**, 682
- Nielsen D. M., Ridgway S. E., De Propriis R., Goto T., 2012, *ApJ*, **761**, L16
- Oppenheimer B. D., Davé R., Kereš D., et al., 2010, *MNRAS*, **406**, 2325
- Panuzzo P., Vega O., Bressan A., et al., 2007, *ApJ*, **656**, 206
- Peletier R. F., Kutdemir E., van der Wolk G., et al., 2012, *MNRAS*, **419**, 2031
- Piovan L., Tantaló R., Chiosi C., 2003, *A&A*, **408**, 559
- Qu Y., Di Matteo P., Lehnert M., van Driel W., Jog C. J., 2010, *A&A*, **515**, A11
- Quintero A. D., Hogg D. W., Blanton M. R., et al., 2004, *ApJ*, **602**, 190
- Rasmussen J., Ponman T. J., Verdes-Montenegro L., Yun M. S., Borthakur S., 2008, *MNRAS*, **388**, 1245
- Rich J. A., Kewley L. J., Dopita M. A., 2011, *ApJ*, **734**, 87
- Richards G. T., Lacy M., Storrie-Lombardi L. J., et al., 2006, *ApJS*, **166**, 470
- Roseboom I. G., Oliver S., Farrah D., 2009, *ApJ*, **699**, L1
- Rowlands K., Wild V., Nesvadba N., et al., 2015, *MNRAS*, **448**, 258
- Sajina A., Lacy M., Scott D., 2005, *ApJ*, **621**, 256
- Sajina A., Yan L., Fadda D., Dasyra K., Huynh M., 2012, *ApJ*, **757**, 13
- Sarzi M., Shields J. C., Schawinski K., et al., 2010, *MNRAS*, **402**, 2187
- Schawinski K., Thomas D., Sarzi M., et al., 2007, *MNRAS*, **382**, 1415
- Schawinski K., Urry C. M., Virani S., et al., 2010, *ApJ*, **711**, 284
- Schawinski K., Urry C. M., Simmons B. D., et al., 2014, *MNRAS*, **440**, 889
- Shin M.-S., Strauss M. A., Tojeiro R., 2011, *MNRAS*, **410**, 1583
- Silk J., Rees M. J., 1998, *A&A*, **331**, L1
- Silva L., Granato G. L., Bressan A., Danese L., 1998, *ApJ*, **509**, 103
- Skrutskie M. F., Cutri R. M., Stiening R., et al., 2006, *AJ*, **131**, 1163
- Smith J. D. T., Draine B. T., Dale D. A., et al., 2007, *ApJ*, **656**, 770
- Spergel D. N., Bean R., Doré O., et al., 2007, *ApJS*, **170**, 377
- Springel V., Di Matteo T., Hernquist L., 2005, *ApJ*, **620**, L79
- Strateva I., Ivezić Ž., Knapp G. R., et al., 2001, *AJ*, **122**, 1861
- Sturm E., Lutz D., Tran D., et al., 2000, *A&A*, **358**, 481
- Sturm E., González-Alfonso E., Veilleux S., et al., 2011, *ApJ*, **733**, L16
- Suh K.-W., Kwon Y.-J., 2011, *MNRAS*, **417**, 3047
- Taylor M. B., 2005, in Shopbell P., Britton M., Ebert R., eds, *Astronomical Society of the Pacific Conference Series Vol. 347, Astronomical Data Analysis Software and Systems XIV*. p. 29
- Temple P., Brighenti F., Mathews W. G., 2007, *ApJ*, **660**, 1215
- Tinsley B. M., 1978, *ApJ*, **222**, 14
- Toomre A., Toomre J., 1972, *ApJ*, **178**, 623
- Trump J. R., Sun M., Zeimann G. R., et al., 2015, *ApJ*, **811**, 26
- Utomo D., Kriek M., Labbé I., Conroy C., Fumagalli M., 2014, *ApJ*, **783**, L30
- Vazdekis A., Sánchez-Blázquez P., Falcón-Barroso J., et al., 2010, *MNRAS*, **404**, 1639
- Vega O., Bressan A., Panuzzo P., et al., 2010, *ApJ*, **721**, 1090
- Verdes-Montenegro L., Yun M. S., Williams B. A., et al., 2001, *A&A*, **377**, 812
- Wild V., Almaini O., Cirasuolo M., et al., 2014, *MNRAS*, **440**, 1880
- Willett K. W., Lintott C. J., Bamford S. P., et al., 2013, *MNRAS*, **435**, 2835
- Wright E. L., Eisenhardt P. R. M., Mainzer A. K., et al., 2010, *AJ*, **140**, 1868
- Xilouris E. M., Madden S. C., Galliano F., Vigroux L., Sauvage M., 2004, *A&A*, **416**, 41
- Yan R., Newman J. A., Faber S. M., et al., 2006, *ApJ*, **648**, 281
- Yang Y., Tremonti C. A., Zabludoff A. I., Zaritsky D., 2006, *ApJ*, **646**, L33
- Yesuf H. M., Faber S. M., Trump J. R., et al., 2014, *ApJ*, **792**, 84
- Young L. M., Scott N., Serra P., et al., 2014, *MNRAS*, **444**, 3408
- Zabludoff A. I., Mulchaey J. S., 1998, *ApJ*, **496**, 39
- Zabludoff A. I., Zaritsky D., Lin H., et al., 1996, *ApJ*, **466**, 104
- Zakamska N. L., Hamann F., Pâris I., et al., 2016, *MNRAS*, **459**, 3144
- Zibetti S., Gallazzi A., Charlot S., Pierini D., Pasquali A., 2013, *MNRAS*, **428**, 1479
- da Cunha E., Charlot S., Elbaz D., 2008, *MNRAS*, **388**, 1595
- van der Wolk G., 2011, PhD thesis, Groningen

parison samples. The code we used is called MAGPHYS and it is described analytically in da Cunha et al. (2008). It is based on the global energy balance between the energy absorbed in the UV and re-emitted in the IR, and adopts a Bayesian ap-

APPENDIX

A. FITTING THE SPECTRAL ENERGY DISTRIBUTIONS

We performed UV to mid-IR SED fitting to estimate the physical properties of the galaxies both in our and the com-

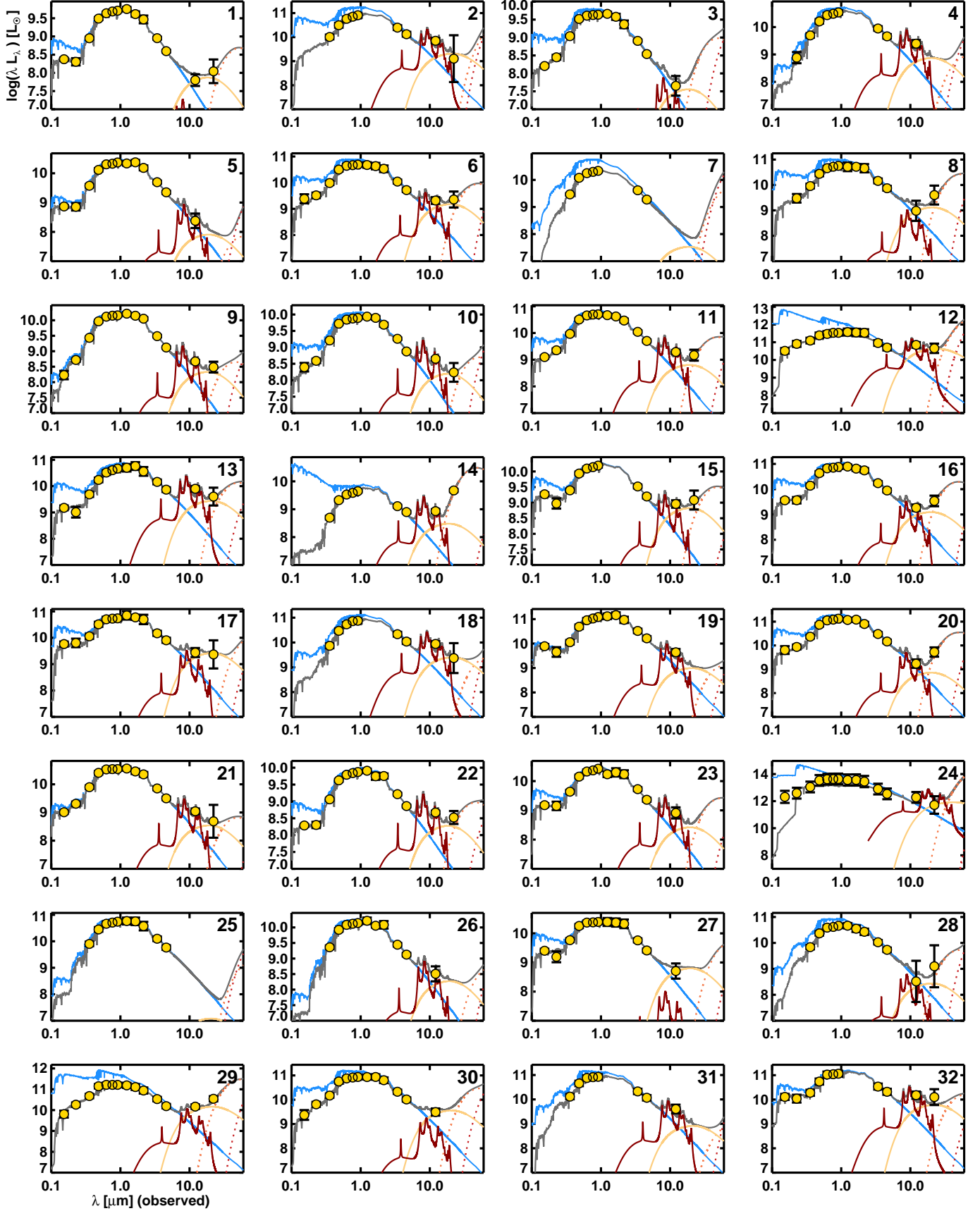


Figure A1. MAGPHYS models of the extended post-starburst galaxies. The yellow points are the observed photometric measurements for each post-starburst. The (unattenuated) stellar model is shown as a blue line. The hot (peach), warm (dotted salmon), and cold (dotted red) power laws are shown, as well as the expected PAH (maroon) emission. The complete fitted model is the dark gray line.

proach which draws from a large library of random models encompassing many parameter combinations, such as the star formation histories, metallicities and dust properties. The theoretical stellar models are computed by the [Bruzual & Charlot \(2003\)](#) population synthesis code, using the initial mass function presented in [Chabrier \(2003\)](#), whereas the dust models are from [Charlot & Fall \(2000\)](#). The code compares the theoretical models with the observed SED of each galaxy and computes the χ^2 value in order to build a probability distribution function (PDF) of each parameter. The final value of each parameter is thus the mean value of the PDF and the uncertainty associated is the given by the 16th and 84th percentiles of the distribution.

MAGPHYS fits multiple components to the re-emitted IR of each galaxy’s SED, including PAH emission, two mid-IR dust components: hot ($T_{\text{dust}} = 130$ or 250 K components) and one warm ($T_{\text{dust}} = 30\text{--}60$ K) component, and finally a cold dust component. Figure A1 shows the SEDs and MAGPHYS fits to all 2MASS XSC post-starbursts. In the majority of cases, the MAGPHYS fits are good, and are better in cases where both 12 and $22\mu\text{m}$ emission is detected. The stellar (blue), PAH (maroon), and hot (peach) dust luminosities combine for the composite model (gray), which are shown in the panels in Figure A1.

B. COMPARISON SAMPLE SELECTION

The comparison samples for the spirals and early-type galaxies used originate from the Galaxy Zoo project ([Lintott et al. 2008, 2011](#)). The AGN sub-selection within Galaxy Zoo originates from [Schawinski et al. \(2010\)](#). The objects directly modeled were selected randomly from the corresponding catalogs. All objects are required to have available SDSS spectroscopic redshift and photometry in SDSS Data Release 9 ([Abazajian et al. 2009](#)).

The early-type galaxy and spiral samples were chosen from the Galaxy Zoo Data Release 2 catalog ([Willett et al. 2013](#)) having the corresponding morphological classifications (not being classified as AGN-hosting). They contain 232 and 194 galaxies respectively.

The AGN sample was chosen from the AGN Host Galaxies catalog ([Schawinski et al. 2010](#)) and comprises 392 AGN-hosting galaxies. This catalog contains a volume-limited sample ($0.02 < z < 0.05$, $M_z < -19.5$ AB) with emission line classifications consistent to those of AGN hosting galaxies.

The UV data were obtained from the Galaxy Evolution Explorer All Sky Survey Data Release 6 ([Morrissey et al. 2007](#)), resulting in far-ultraviolet (FUV; 1540\AA) and near-ultraviolet (NUV; 2300\AA) measurements. All photometric measurements were automatically performed using SEXTRACTOR (see [Bertin & Arnouts 1996](#)). Finally, we used the

WISE mid-IR photometry from [Lang et al. \(2016\)](#). These authors performed the “forced photometry” technique in a consistent set of sources between SDSS and WISE, taking advantage of the high resolution of SDSS images to interpret the WISE data.

C. CALCULATING THE POSSIBLE EDDINGTON RATIOS FROM THE HOT DUST LUMINOSITIES

To determine the possible Eddington ratios of the post-starbursts, we derived values for black hole masses and potential AGN luminosities. We first obtained estimates of the stellar velocity dispersions from SDSS DR9 ([Ahn et al. 2012](#)) for the 190 2MASS XSC post-starbursts. We then estimated black hole masses using the $M_\bullet\text{--}\sigma$ relation from formula 7 in [Kormendy & Ho \(2013\)](#). The Eddington luminosity was then derived using $L_{\text{Edd}}/L_\odot = 3.2 \times 10^4 M_\bullet/M_\odot$. The possible bolometric luminosities represented by these post-starbursts were estimated by assuming that 100% of the MAGPHYS-derived hot dust luminosity originated from an AGN ([Sajina et al. 2005](#); [Richards et al. 2006](#); [Lusso et al. 2013](#)), thus we can estimate the bolometric luminosity of the AGN to be approximately $5 \times L_{\text{hot}}$.

Figure C1 shows the Eddington ratio distribution for the post-starbursts, assuming that the entire hot dust luminosity originates from an AGN. The derived Eddington ratios range between 10^{-4} and 10^{-2} , with a peak around 10^{-3} . This firmly places the post-starbursts into the low-luminosity regime, consistent with the findings of [Brown et al. \(2009\)](#) and [De Propriis & Melnick \(2014\)](#), based on X-ray measurements.

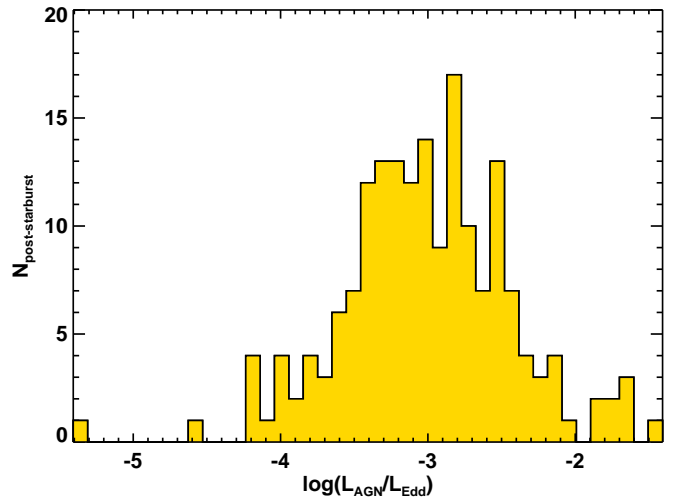


Figure C1. The estimated upper limits to the Eddington ratios represented by the mid-IR hot dust luminosities of the post-starbursts. The estimated ratios firmly place the potential AGNs in post-starbursts into the low-luminosity AGN regime.